Fine-Resolution Silicon Photonic Wavelength-Selective Switch Using Hybrid Multimode Racetrack Resonators

Lucas M. Cohen, Saleha Fatema, Vivek V. Wankhade, Navin B. Lingaraju, Bohan Zhang, Deniz Onural, Miloš Popović, *Senior Member, IEEE*, and Andrew M. Weiner, *Life Fellow, IEEE*

***Abstract*—In this work, we describe a procedure for synthesizing racetrack resonators with large quality factors and apply it to realize a multi-channel wavelength-selective switch (WSS) on a silicon photonic chip. We first determine the contribution of each component primitive to propagation loss in a racetrack resonator and use this data to develop a model for the frequency response of arbitrary order, coupled-racetrack channel dropping filters. We design second-order racetrack filters based on this model and cascade multiple such filters to form a 1×7 WSS. We find good agreement between our model and device performance with second-order racetrack that have ≈ 1 dB of drop-port loss, ≈ 2 GHz FWHM linewidth, and low optical crosstalk due to the quick filter roll-off of ≈ 5.3 dB/ GHz. Using a control algorithm, we show three-channel operation of our WSS with a channel spacing of only 10 GHz. Owing to the high quality factor and quick roll-off of our filter design, adjacent channel crosstalk is measured to be < -25 dB for channels spaced on a 10 GHz grid. As a further demonstration, we use five of seven WSS channels to perform a demultiplexing operation on both an 8 GHz and a 10 GHz grid. These results suggest that a low-loss WSS with fine channel resolution can be realized in a scalable manner using the silicon photonics platform.**

***Index Terms*—Wavelength-selective switch, wavelength-division multiplexing, telecommunications, microresonators, silicon photonics.**

I. Introduction

As INTERNET traffic volume and the demand for data increase, existing optical transport architectures will require hardware upgrades for the improvement of transmission capacity and capabilities of optical networks. Reconfigurable optical add-drop multiplexers (ROADMs) are a critical building block of optical networks, enabling flexibility in wavelength routing and assignment between users on an optical network. ROADMs are comprised principally of a wavelength-selective switch (WSS, shown schematically in Fig. 1(a)), and WSSs that are actively deployed today are most commonly based on diffraction grating-based spectral dispersers and liquid crystal-on-silicon (LCoS) technology [1]. Although well suited to optical network requirements, such WSSs require assembly of bulk or micro-optic components, are typically limited to spectral resolutions at ca. 10 GHz and above, and induce excessive optical loss especially when modified to perform filtering operations at unusually fine spectral resolutions in the few GHz range [2]. Moreover, such systems, often realized in free space, are limited to using spatial filtering methods that can only be altered mechanically and are difficult to control.

Chip-scale WSSs that use on-chip microresonators are a promising solution due to their high selectivity, compact footprint, and simple operation [4], [5]. Coupling multiple microresonators to each other enables the construction of higher-order filters with flat-band responses and increased selectivity. When integrated with microheaters, the refractive index can be changed locally, allowing for precise control over filter characteristics like center frequency, bandwidth, and filter shape. The scalability, affordability, and comprehensive component catalog offered by silicon photonics technology (SiP) further underscore its suitability for implementing a SiP WSS, thereby attracting considerable research interest [6], [7]. An M input spatial channel, L output wavelength channel $M\times L$ WSS [8], a flexible-grid WSS [9], and even an M input spatial channel, N output spatial channel,L wavelength channel/port$M\times N\times L$ WSS [10] have been demonstrated using microresonators with SiP technology. However, current demonstrations have used microresonators with relatively low quality factors, rendering them incapable of meeting the fine-resolution requirements that could be asked of ROADMs in the future [11]. For example, over the past decade there has been a push towards utilizing optical superchannels to improve spectral efficiency and total throughput in an optical network [12], [13]. There are scenarios in which subchannel add/drop capabilities within a superchannel are desirable. Performing these functions optically has a

Manuscript received 20 September 2023; revised 20 January 2024 and 22 February 2024; accepted 24 February 2024. Date of publication 28 February 2024; date of current version 8 July 2024. This work was supported in part by NSF under Grant 2034019-ECCS, in part by AFRL under Grant FA8750-20-P-1705, and in part by STTR through Freedom Photonics. *(Corresponding author: Lucas M. Cohen.)*

Lucas M. Cohen, Saleha Fatema, Vivek V. Wankhade, and Andrew M. Weiner are with the Purdue Quantum Science and Engineering Institute and the Elmore Family School of Electrical and Computer Engineering, Purdue University, West Lafayette, IN 47907 USA (e-mail: cohen26@purdue.edu).

Navin B. Lingaraju is with the SRI International, Arlington, VA 22209 USA, and also with the John Hopkins University Applied Physics Laboratory, Laurel, MD 20723 USA.

Bohan Zhang, Deniz Onural, and Miloš Popović are with the Department of Electrical and Computer Engineering, Boston University, Boston, MA 02215 USA.

Color versions of one or more figures in this article are available at https://doi.org/10.1109/JLT.2024.3371161.

Digital Object Identifier 10.1109/JLT.2024.3371161

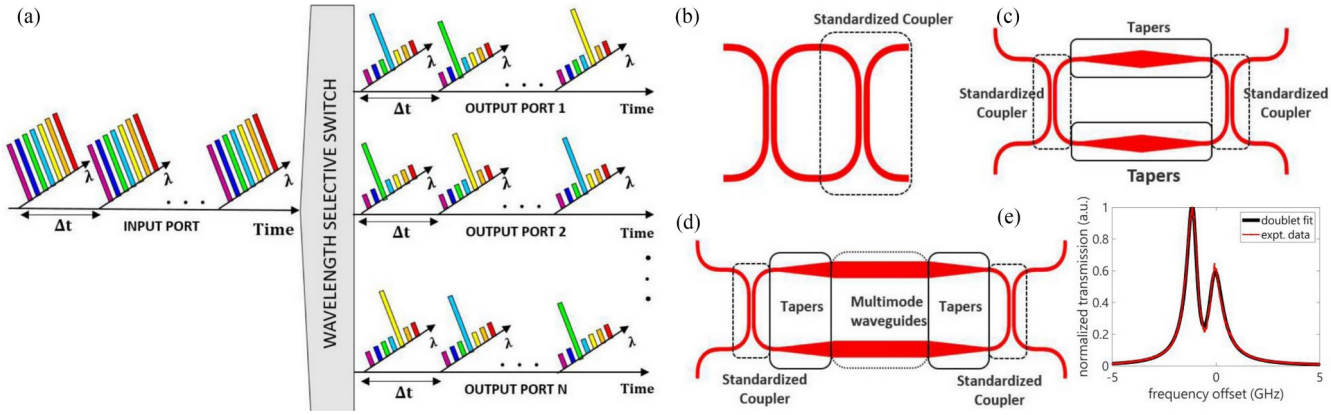

Fig. 1. (a) Conceptual diagram of a 3-channel WSS. (b) Weakly coupled resonator to characterize standardized couplers. (c) Weakly coupled resonator to characterize adiabatic tapers. (d) Full hybrid multimode racetrack filter comprised of single-mode standardized couplers, adiabatic single to multimode waveguide tapers, and multimode waveguides. (e) Example spectral response from a weakly coupled structure with the geometry of Fig. 1(b) with a doublet resonance mode and fit.

number of potential benefits to the network, but it requires high-selectivity filtering (resolution at the single GHz level) to e.g. add guard bands between adjacent subchannels as well as to assist in picking out the subchannel. Although there have been impressive demonstrations of such hyperfine resolution filtering [14], [15], [16], [17], [18], such demonstrations rely on substantially more complex optical setups or exotic components and are subject to increased insertion loss, as mentioned above.

Selective wavelength filtering (sub-GHz linewidths) is also important in applications like quantum information science and microwave photonics. In particular, many view modular architectures as essential to the scale-up of quantum computing systems, where communications and entanglement between individual computational modules is mediated by photons [19]. These photons, which must interface with matter-based qubits, will have linewidths on the order of 10 s to 100 s of MHz. Consequently, low-loss and narrowband filters can help selectively manipulate or route these modes over local area or larger networks [20]. Microwave photonics, the science of processing radiofrequency signals in the optical domain [21], similarly requires the ability to control and isolate narrowband optical signals with low loss in order to realize systems with low noise figures. Such systems can be harnessed for applications like abritrary waveform generation and shaping of low-repetition rate combs, among others [22].

In this paper, we propose and experimentally demonstrate a multi-channel WSS using racetrack resonators with a hybrid geometry that includes wide waveguide segments to make possible optical filtering at a fine-resolution. We first develop a methodology for the robust modeling of arbitrary order coupled-racetrack devices using experimental data. The developed model shows good agreement with experimental results and enables first-time-right designs of narrowband filters. Next, we use the model to design a 1×7 WSS with a second-order filter response with ≈ 1 dB of drop-port loss, 2 GHz FWHM channel linewidth, and 5.3 dB / GHz of roll-off, and we demonstrate WSS operation using 3 filter channels. As our current device does not offer tunable channel bandwidth or attenuation, we alternatively term the device a *fine-resolution wavelength demultiplexer* and show 1×5 operation on both 8 and 10 GHz frequency grids. A subset of results from this manuscript was presented at the IEEE Photonics Conference [23] and Conference on Lasers and Electro-Optics [24]. Here, we significantly extend the design methodology and results from previous proceedings. Coupled with recent advances in on-chip optical I/O [25], oour work takes a step towards showing the SiP platform is capable of meeting the fine-resolution filtering requirements of future-generation optical networks.

The remainder of this paper is outlined as follows. In Section II, we discuss our empirical method to design first-time-right arbitrary order racetrack filters. In Section III we use this method to design a 1×7 WSS with second-order racetrack filters. As an example, we then use the system in both a 1×3 WSS and 1×5 demultiplexer configuration and discuss the performance in detail. In Section IV, we explore opportunities for improvement, and we conclude with a summary in Section V.

II. Filter Model

We focus on racetrack filters comprised of three elements: a single-mode coupling region, adiabatic tapers from 0.5 μm wide to 2 μm wide waveguides, and 2 μm wide multimode waveguides. Adiabatic tapers facilitate the propagation of the fundamental mode from a single-mode waveguide to multimode without excitation or loss to higher-order modes. The multimode waveguide, when operated in the fundamental mode, significantly reduces the dominant loss mechanism for SiP waveguides of field-sidewall overlap, thus providing low-loss [26]. For sufficiently long multimode waveguide sections, the average round-trip loss through the racetrack is dominated by this element, thereby enabling one to flexibly tune the resonator's quality factor with the multimode waveguide length [5].

To characterize the loss contributions of each element of our racetrack resonators, we design structures on a full-stack active multi-project wafer (MPW) run [23]. These structures follow the weakly-coupled cavity method [27] in which a resonator is sufficiently weakly coupled to bus waveguides such that the linewidth of its frequency response is dominated by the intrinsic

TABLE I
EXTRACTED LOSS FOR RACETRACK RESONATORS AND INDIVIDUAL SUBCOMPONENTS

Device	Structure of Interest (Units in μm)	Resonator Intrinsic Q	Resonator Average Loss (dB/cm)	Structure Loss (dB)	Structure Average Loss (dB/cm)
Weakly Coupled Microring	Ring Resonator, ($R = 20$)	4.37×10^5	1.8	0.0110	1.8
Fig. 1(b)	Standardized Coupler $R_{\min} = 3$	1.43×10^5	5.43	0.0099	5.43
Fig. 1(b)	Standardized Coupler $R_{\min} = 4$	2.33×10^5	3.32	0.0075	3.32
Fig. 1(b)	Standardized Coupler $R_{\min} = 5$	3.29×10^5	2.33	0.0064	2.33
Fig. 1(c)	Linear Taper, Length = 30	3.26×10^5	2.16	0.0062	2.09
Fig. 1(c)	Linear Taper, Length = 50	5.57×10^5	1.24	0.0047	0.95
Fig. 1(c)	Linear Taper, Length = 100	8.26×10^5	0.82	0.0062	0.62
Fig. 1(c)	Linear Taper, Length = 200	9.68×10^5	0.70	0.0117	0.59
Fig. 1(d)	Fourier Taper*, Length = 11.36	1.64×10^6	0.40	0.0034	3.01
Fig. 1(d)	Multimode Waveguide, Length = 700	1.67×10^6	0.40	0.0170	0.24
Fig. 1(d)	Multimode Waveguide, Length = 1200	1.89×10^6	0.35	0.0300	0.25

$*$ Measured from device of Fig. 1(d) with 700 μm long multimode waveguides.

loss of the resonator as opposed to the external losses from the coupling to the bus waveguides. A careful balance must be achieved so as to be sufficiently weakly coupled with the resonator yet coupled enough to have a strong signal at the drop port. In this way, the loss contributions from an arbitrary component can be measured without taking up an excessive footprint on the chip.

There are three classes of test structures, as shown in Fig. 1(b)–(d). Each consists of a resonator comprised of a pair of what we term *standardized couplers* that sandwich either two pairs of tapers or two pairs of tapers and a pair of multimode waveguides that we want to characterize. The standardized coupler is a single-mode region formed by two 90 $^\circ$ graduated radii bends with a 5 μm long straight waveguide in between. This straight coupling section provides a long interaction region to realize sufficiently high bus-racetrack coupling even for large bus-racetrack gaps, which are better tolerated by the fabrication process and can also lead to reduced coupling losses. The 90 $^\circ$ bends are hybrid structures comprising two Euler curves and a circular arc of constant radius that matches the minimum radius of the Euler curves [28]. In this way, the Euler curve reduces mode mismatch loss from the interface with a straight waveguide, while the circular section minimizes the footprint of the composite curve. These standardized couplers simplify the formation of coupled-resonator designs since the physical coupling structure is identical for both bus-resonator and resonator-resonator couplings.

These test structures were fabricated through an active MPW run through AIM Photonics on 220 nm-thick silicon-on-insulator (SOI) wafers [29]. There are devices for three variations of the standardized coupler - variants with minimum radii ($R_{\min}$) of 3μm, 4μm, and 5μm. Our test devices covered a range of linear taper lengths from 30μm to 200μm. Besides the linear tapers, we also included a set of full racetracks (Fig 1(d)) with adiabatic tapers where the tapered shape synthesized is based on a Fourier modal method so that the taper length is minimized for a given loss [30], [31]. Also, we have two devices to measure 2 μm wide waveguide loss with different 2 μm waveguide lengths of 700μm and 1200μm. These devices contain a 100μm long linear taper to expand the waveguide to a 2 μm width. Finally, we have one test device with a weakly coupled circular microring resonator of radius $R = 20$ μm with 0.5 μm wide waveguides to gather a baseline single-mode waveguide loss for reference. All the test devices are designed with identical input and drop bus coupling gaps, and we vary this gap over a broad range such that we can successfully characterize a weakly coupled device. A standard SMF-28 optical fiber array with an angled facet adjusted by an external polarization controller is used to test devices.

A representative spectrum with fitting from a single weakly-coupled device with the structure of Fig. 1(b) is shown in Fig 1(e). The average propagation loss of the racetrack resonator can be computed from the fitted quality factor and device parameters. The results are shown in Table I, where we tabulate the intrinsic quality factor of racetrack resonators comprising different combinations of sub-components, as well as break out the contribution to loss from the sub-component or structure of interest [23]. In the table, the resonator intrinsic Q and average loss are computed directly from the frequency response of the device, while the contribution to loss from each sub-component is isolated after the contributions from previously characterized sub-components are removed. Three different die are tested to accumulate the results, except for the standardized couplers where seven die are used.

We see that standardized couplers with $R_{\min} = 5$ μm offered not only the lowest average loss, but also the lowest total structure loss, making them a good choice for multimode racetrack filters with high quality factors. For the linear tapers, a clear decrease in the taper's average loss is measured as the length of the taper increases, while the structure loss shows a more complicated trend. From the data in Table I, we see that the Fourier tapers are measured to have the largest average loss but have the lowest insertion loss owing to their short length (11.36 μm). Finally, we computed the losses of 2 μm-wide multimode waveguides of different lengths. Because of their significant path length, they account for the dominant loss contribution in the racetrack yet their average loss of $\approx$ 0.25 dB/cm is significantly lower than what we measure for a 0.5 μm wide single mode waveguide of 1.8 dB/cm.

In Fig. 2(a), we plot the power coupling ratio between standardized couplers of $R_{\min} = 5$ μm as a function of the gap between them measured for the TE polarization. We are able to extract such information because of our variation in standardized coupler gaps from our test devices. Full 3-D finite-difference

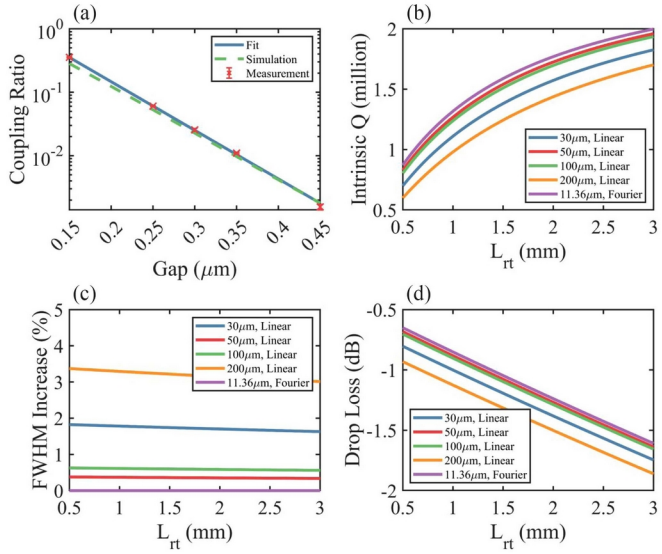

Fig. 2. (a) Simulation and experimentally extracted cross coupling ratio versus gap for standardized couplers with $R_{min} = 5\,\mu$m. Simulated (b) intrinsic quality factor, (c) percent increase in 3 dB linewidth relative to racetrack with Fourier tapers, (d) drop-port insertion loss versus round-trip racetrack resonator length for all measured taper variants, respectively, and assuming a constant power coupling of 5%, respectively.

time domain (FDTD) simulation results show good agreement with what we extract from measurement, with a slight underestimate in simulation at smaller gaps ($< 0.25\,\mu$m).

To quantitatively describe the frequency response of a racetrack comprised of a variation of these subcomponents, we developed a model using our experimentally extracted data. The model relies on well-known analytical formulas [4], [5] and is scalable to higher-order coupled racetrack structures in order to increase the filter roll-off [32]. An example of data from our model is shown in Fig. 2 for a first-order racetrack designed with input and output bus waveguides having a coupling ratio of 5% (a gap near 0.25 μm using our data from Fig. 2(a)). We use the standardized coupler with $R_{min} = 5\,\mu$m and plot a few useful quantities for a single resonance mode at $\lambda = 1550$ nm for all our measured taper variants. The round-trip length of the racetrack is held fixed in the simulations by modifying the length of the multimode waveguide and therefore, for all taper variants to within a small error, the free spectral range (FSR) of the racetrack at a particular round-trip length is a constant. A group index of 3.5 is chosen in simulation and is near the measured value presented in Section III.

From Fig. 2, we see that the Fourier tapers should be used to maximize the quality factor of the racetrack. Interestingly, the intrinsic quality factor increases for linear tapers as we increase the length from 30 μm to 50 μm, then it decreases slightly at 100 μm and more rapidly for 200 μm. From this trend, we reason that the optimal linear taper length is somewhere between 50 and 100 μm long. Longer than that and the taper expands too slowly for it to have a loss advantage. For all tapers, as the round-trip length increases, the resonance mode linewidth asymptotes towards a value around 500 MHz where light propagation in the racetrack becomes the dominant source of cavity loss. This value is based on our fixed coupling coefficient used in the simulation. However, the drop-port loss also increases quickly as the racetrack is now larger and has a greater total round-trip loss.

When making conclusions from our model towards designing useable racetrack devices, it is necessary to recognize the tradeoffs involving the resonator's FSR and its quality factor [4]. In particular, the intrinsic quality factor of a resonator is $Q_i = 2\pi n_g/\alpha_{avg}\lambda$ where n_g, α_{avg}, and λ are the group index, length-averaged round-trip loss, and resonance wavelength. The length-averaged round-trip loss can be expressed for our resonators as

$$\alpha_{avg} = \frac{\sum_{i=0}^{n} L_i \alpha_i}{\sum_{i=0}^{n} L_i}. \tag{1}$$

where α_i and L_i are the length-averaged loss and the length for the i^{th} subcomponent of the resonator. In this form, it is clear that as the length of a particular component is increased, its contribution to the average loss of the resonator is as well. However, the FSR of the resonator, $\Delta\nu = c/\sum_{i=0}^{n} L_i n_{g,i}$, is inversely proportional to its round-trip length. Hence, increasing the length of the lowest-loss component does indeed increase the quality factor of the resonator but at the cost of a reduced FSR, limiting the usable bandwidth of the device. Obviously, each parameter of the racetrack must be carefully chosen with the design application in mind.

III. WSS Design and Operation

A 1×N wavelength selective switch (schematically shown in Fig. 1(a)) is a device which takes as input a broadband optical field and, in a re-programmable fashion, separates and routes distinct slices of that input spectrum to N distinct outputs. Our designed on-chip WSS structure is shown in 3(b). We use seven identical second-order racetrack filters coupled to a common input bus waveguide with unique drop-port I/O to form a 1 ×7 WSS. Our racetrack filters are designed following the methodology described in Section II, and we choose second-order structures for the increase in roll-off off of resonance. The bus-racetrack and racetrack-racetrack standardized coupler gaps are set to ≈ 190 nm and 370 nm for power coupling coefficients of ≈ 18 and 0.8 %, respectively. In this way, we can pack filter channels more closely together than a single-order structure for the same level of inter-channel optical crosstalk. Each individual racetrack of the filter has the same round-trip length of ≈ 1500 μm, uses Fourier tapers, and standardized couplers with $R_{min} = 5\,\mu$m. Standardized coupler gaps are set to achieve a flat passband frequency response with the smallest possible linewidth with the constraint that drop port loss does not exceed 1 dB.

The WSS chips were fabricated through an AIM Photonics MPW program at the SUNY Polytechnic Institute in a state-of-the-art 300 mm facility. Photonics-grade 220 nm thick SOI wafers with a thick buried oxide are used with 193 nm immersion lithography to define silicon optical waveguiding structures. Embedded microheaters in the form of doped silicon slabs with various vias and metal interconnect layers for electrical

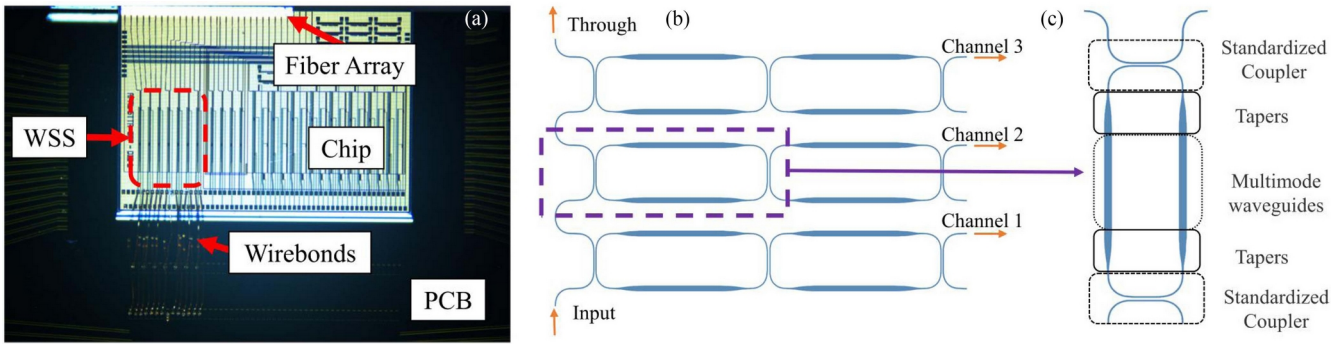

Fig. 3. (a) Top-down microscope view of the silicon photonic WSS package. (b) Layout of the on-chip WSS. (c) Zoom-in view of an individual racetrack of the coupled-resonator filter.

contact are placed 1.25 μm from the optical waveguide in each racetrack resonator. In this way, an injected current in the slab can generate heat via the Joule heating effect to locally modify the refractive index and tune the racetrack resonance through silicon's thermo-optic effect.

The fabricated chips were sent out for electrical wirebonding and packaging at the testing and packaging (TAP) facilities at Rochester Institute of Technology using a custom-developed electronic interposer and printed circuit board (PCB). To control each of the 7 WSS second-order racetrack filters, 21 wirebond connections were made. The full footprint of the 1 ×7 WSS is about 4 mm by 1.5 mm but can be significantly reduced by placing electrical and optical I/O more compactly. Excluding I/O, the 1x7 WSS occupies a footprint of 1.5 mm by 1.5 mm. The wirebonded package was placed on a custom temperature controlled chuck for compatibility with our optical probe station. A top-down view of the wirebonded chip package is shown in Fig. 3(a). The WSS was tested using a 16 channel SMF-28 optical fiber array with a flat facet fed by an Agilent 81632 A tunable laser source with an external polarization controller. For thermal tuning, we use a 64-channel source measurement unit (SMU) with electronic cabling to interface with our package.

We first characterize the individual filter response of our WSS by sending laser light into the common through port and monitoring the output power at the common through port and drop port of channel 1. If we sweep the laser wavelength as we apply increasing electrical power to the thermo-optic heaters of a single racetrack of the filter, we can find the thermal state where the two resonators comprising the second-order filter are optically aligned. The final tuned state of the filter at a wavelength near 1550 nm is shown in Fig. 4 along with a simulation using our model. We see good agreement between the two, further indicating the utility of the model. The passband shows a flat response with a $\approx$ 2.1 GHz linewidth and 1 dB insertion loss. The FSR of the filter is about 54.5 GHz from which we extract an average group index of 3.54. The filter linewidth deviates $<$ 150MHz over a measured bandwidth of 10 nm, and all devices perform as expected irrespective of the tested die [33].

The performance of the second-order filter was also characterized over a range input optical powers to elucidate the impact of thermal effects [34] and nonlinear absorption [35]

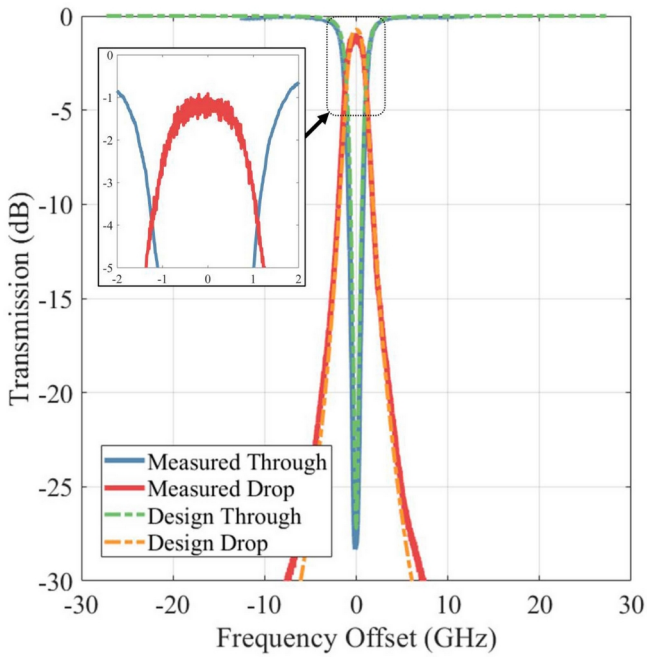

Fig. 4. Measured optical frequency response for a single mode of the filter at $\lambda = 1550$ nm plotted with the designed filter response using our model developed in Section II. The inset shows the flat-top passband.

on linewidth. Fig. 5 shows the frequency response of this filter for on-chip input powers of -6.0 dBm, -0.2 dBm, and 4.1 dBm. The inset of Fig. 5 shows the change in filter linewidth for nine different on-chip input power levels and we observe broadening that increases linearly with optical power in dBm over a range the spans input powers that span -6.0 dBm to 4.1 dBm. For powers above 4.1 dBm we began to observe bistability in the filter response.

To use our system as a WSS, we need to tune each filter to its optimal response and then align them on a hypothetical frequency grid. To this end, we developed a Python algorithm with open-source libraries. In the algorithm, a continuous-wave laser is input into the chip and repeatedly tuned between each frequency in the grid. An optical power meter measures the transmitted power at the common through port while a multi-objective minimization routine using the NGSAII sampler from the

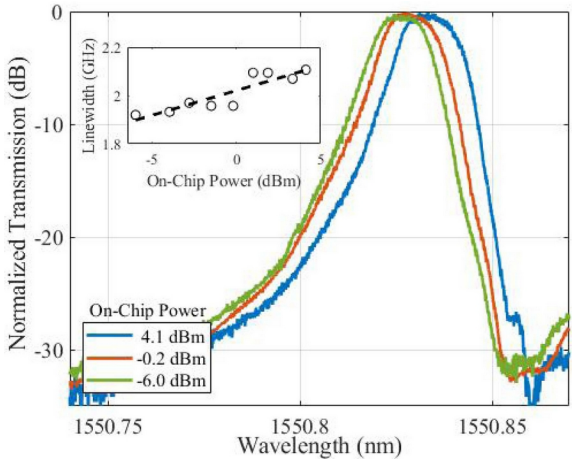

Fig. 5. Frequency of a second-order racetrack filter for different on-chip input powers. The spectra are normalized with respect to the peak of each passband. The inset shows the change in the 3 dB linewidth of the filter as a function of optical power coupled onto the chip.

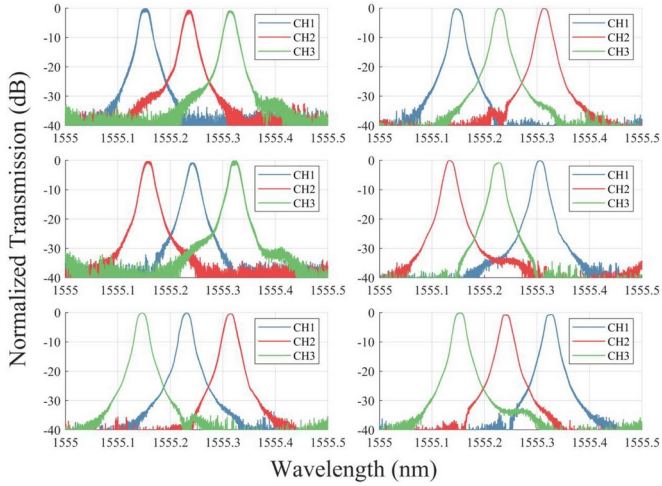

Fig. 6. Spectra from the six permutations of the three channel WSS as measured from a swept tunable laser source. For each permutation, traces are normalized to the channel with maximum transmission.

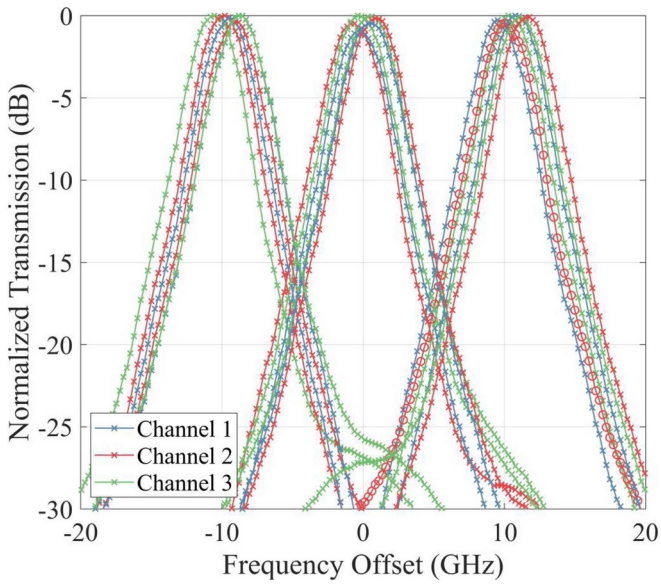

Fig. 7. Overlayed spectra from the six permutations of the three-channel WSS as measured from an OSA. For each permutation, traces are normalized to the channel with maximum transmission. The input of the WSS is a broadband, flat ASE spectrum from an EDFA.

open-source library Optuna [36] drives the microheaters appropriately – even in the presence of mutual thermal crosstalk – to minimize the transmitted optical power at each frequency position. In this way, individual racetracks are optimally tuned to a common resonance mode and shifted to align with the frequency grid at drive states that give the minimum objective function value. For each state of the WSS, filters are first manually tuned to be relatively close to their location on the frequency grid in order to minimize the runtime of the algorithm. A single WSS state is then gathered in roughly 30 minutes using our serially updated electronics. Using an SMU with a faster or parallel update rate would decrease this runtime.

We programmed a three channel subset of our WSS for operation on a 10 GHz spaced grid near 1550 nm. Each channel was aligned to a unique position on this three-point grid [24]. There are six permutations for three channels on this grid, and the spectra for each state taken from a tunable laser sweep are shown in Fig. 6. From the figure, we can clearly see at the center of any channel better than 25 dB dB of isolation from the (both) adjacent channel(s). The average electrical power consumption for each racetrack is $\approx$ 50 mW for thermal tuning. However, racetracks are initially detuned from unused channels to prevent light leakage, contributing overhead to this power budget.

Using the spectra of Fig. 6 measured from a scanned laser, we computed an average detuning from the predefined frequency grid of $\approx 0.8 \pm 0.5$ GHz for each channel in the WSS. To avoid possible wavelength registration errors, which can arise during successive wavelength sweeps from a tunable laser, we perform a single-shot measurement over all frequency channels in a permutation with an optical spectrum analyzer (OSA). For this purpose, we send a broadband amplified spontaneous emission (ASE) spectrum from an erbium-doped fiber amplifier (EDFA) to the input port of our WSS and measure the output of each channel for all permutations with our OSA. An overlay of the measured spectra are shown in Fig. 7 [24]. We see a slight increase in optical crosstalk from the OSA measurement that can be attributed to the 0.01 nm ($\approx$ 1.247 GHz) resolution of our OSA. We compute an average frequency detuning of 0.7 ± 0.1 GHz for each filter of the WSS using our OSA. We also measured a loss variation of $<$ 0.5 dB from the nominal 1 dB drop-port loss for each channel of the WSS using both laser and OSA spectra.

As a final extension of our device, we program the WSS for a 1×5 demultiplexing operation on both an 8 and 10 GHz frequency grid. Operating the WSS with 5 channels would require 5! optimized permutations, which is possible given the need and enough time. However, here we show only a single permutation as an example. The spectra for both 8 and 10 GHz grids are shown in Fig. 8 as measured from a swept tunable laser source. Channels 3, 4, and 5 are the channels used in Figs. 6 and 7 for WSS operation. We see from the blue and

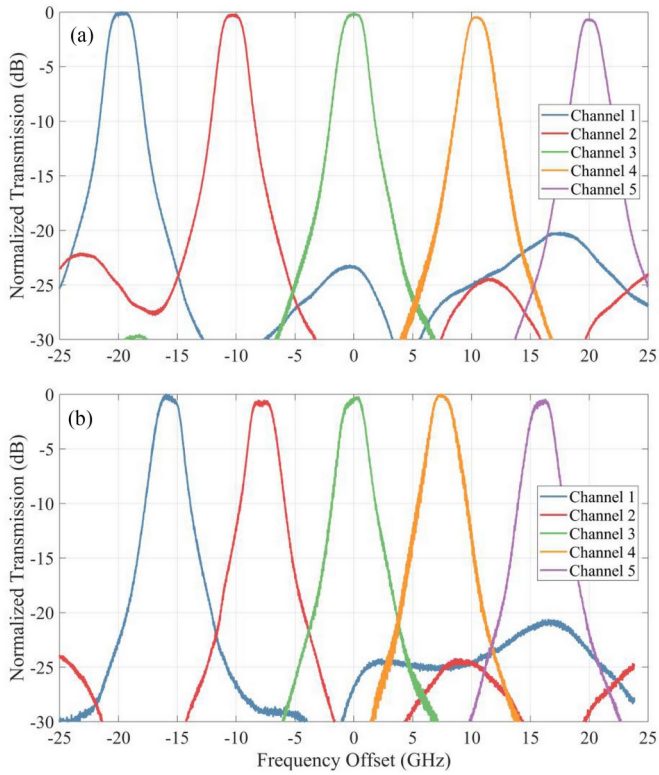

Fig. 8. Measured spectra for the WSS configured as a 1 ×5 demultiplexer as taken from a swept laser source for (a) 10 and (b) 8 GHz grid spacing. The center wavelength for both grids is ≈ 1551 nm. Traces are normalized to the channel with maximum transmission.

red traces that adding channels 1 and 2 for the demultiplexer results in a slight increase in optical crosstalk at both the high and low-frequency region of the spectrum. Nonetheless, the crosstalk for both 8 and 10 GHz spacing remains below <-20 dB in all cases. Besides the crosstalk, we see a transmission variation of <0.75 dB between each channel for both grids.

IV. Discussion

The primary challenges with scaling the high quality devices shown here are: 1) extending the FSR, 2) reducing the electrical power needed for thermal tuning, and 3) developing a robust control solution. Since the quality factor of the racetrack increases with the multimode waveguide length, it is common for the FSR of the high quality devices to be on the order of 10 s of GHz, if not lower. Depending on the spacing, this can present limitations on the maximum number of channels that can be used. A common way of increasing the FSR is by using coupled-resonator structures with different round-trip lengths in a Vernier configuration [37]. This has been shown to extend the operating FSR of the device. Yet it requires significant engineering to get large suppression of the interstitial resonance peaks, among other challenges [38]. Likewise adding frequency dependence to the coupling coefficient in the form of an interferometer could function to extend the FSR of the device [39]. Interferometric coupling could also allow tuning of the filter bandwidth, enabling flex-grid performance with tunable center frequency and bandwidth [40]. However, an interferometer would add an extra phase tuning element because of fabrication imperfections and thus complicate the operation.

Reducing electrical power consumption from thermal tuning can be accomplished in a number of ways. For a demultiplexer, frequency positions of each racetrack can be prebiased in fabrication by adjusting the round-trip path lengths. While thermal tuning would still be required to compensate for variation in fabrication, it would take less power than if racetracks were identical like our design here. Still this method is not effective for a WSS since filters need to be tuned to each position on the frequency grid. Second, by thermal isolation trenching of top and bottom oxide materials as well as removing the silicon substrate, the electrically generated heat can be kept from spreading away from the optical waveguide [41]. Such processes would also help alleviate thermal crosstalk effects further reducing the required electrical power consumption.

A number of control methods could help realize a large-scale on-chip WSS. A common approach to lock microrings to an optical carrier is to monitor the intra-cavity optical power using a photoconductive element embedded within the optical cavity, often in the form of a doped (n, p, or p-n) region of the waveguide [42]. However, this fundamentally leads to excess loss thereby reducing the resonator quality factor. Another scheme uses a contactless probe placed adjacent to a waveguide capable of sensing light in the waveguide by measuring a conductance change induced by free-carriers being generated at the silicon-insulator interface. A low-frequency modulation of an optical carrier can then be detected by the probe and used to lock microrings to a laser even in the presence of multiple laser sources [43], [44]. In a similar vein, low-frequency thermal modulation of a microring has been used to encode a shallow amplitude modulation onto an optical carrier which can, upon photodetection, induce an asymmetric error signal appropriate for frequency locking [45]. As monolithic electronic-photonic systems [46] become increasing available, on-chip control of silicon photonic concepts such as ours may become feasible.

V. Conclusion

In conclusion, the design methodology and results were presented for a WSS implementing high quality factor microresonator filtering elements. The procedure outlined here can be used on any integrated platform to realize first-time-right devices. By tuning parameters of the subcomponents of the high quality racetrack, arbitrary filter responses can be achieved. For our designed WSS, we demonstrate second-order filters with $\approx$ 1 dB of drop-port loss, $\approx$ 2 GHz FWHM linewidth, and quick off-resonance roll-off of ≈ 5.3 dB / GHz. We use our system to experimentally show 3 channel WSS operation on a 10 GHz grid and 5 channel multi/demultiplexer operation on both an 8 and 10 GHz grid, both with <-20 dB of inter-channel optical crosstalk. Using our designed components, higher-order filters can be easily assembled to achieve increased selectivity as required. A flexible grid spacing and channel count can be accommodated for by applying the appropriate amount of electrical power to each racetrack. The performance of our devices shows promise towards realizing fine-resolution filtering in future silicon photonic systems.

ACKNOWLEDGMENT

The authors would like to thank Matthew van Niekerk and Stefan Preble at Rochester Institute of Technology for assistance with wirebonding and package assembly, and Cale Gentry from SRI International for discussions.

REFERENCES

[1] S. Gringeri, B. Basch, V. Shukla, R. Egorov, and T. J. Xia, "Flexible architectures for optical transport nodes and networks," *IEEE Commun. Mag.*, vol. 48, no. 7, pp. 40–50, Jul. 2010.

[2] Y. Ma et al., "Recent progress of wavelength selective switch," *J. Lightw. Technol.*, vol. 39, pp 896–903, 2021.

[3] S. Siew et al., "Review of silicon photonics technology and platform development," *J. Lightw. Technol.*, vol. 39, pp 4374–4389, 2021.

[4] S. Feng et al., "Silicon photonics: From a microresonator perspective," *Laser Photon. Rev.*, vol. 6, pp 145–177, 2012.

[5] W. Bogaerts et al., "Silicon microring resonators," *Laser Photon. Rev.*, vol. 6, pp 47–73, 2012.

[6] X. Tu et al., "State of the art and perspectives on silicon photonic switches," *Micromachines*, vol. 10, 2019, Art. no. 51.

[7] X. Chen, J. Lin, and K. Wang, "A review of silicon-based integrated optical switches," *Laser Photon. Rev.*, vol. 17, 2023, Art. no. 2200571.

[8] C. Zhang et al., "Silicon photonic wavelength-selective switch based on an array of adiabatic elliptical-microrings," *J. Lightw. Technol.*, vol. 41, pp 5660–5667, 2023.

[9] W. Chen et al., "Experimental demonstration of a flexible-grid 1x2 wavelength-selective switch based on silicon microring resonators," *Opt. Lett.*, vol. 44, pp 403–406, 2019.

[10] A. Khope et al., "Multi-wavelength selective crossbar switch," *Opt. Exp.*, vol. 27, pp 5203–5216, 2019.

[11] S. Perrin, "Building a fully flexible optical layer with next-generation ROADMs," White paper from Heavy Reading, 2011.

[12] P. Winzer, D. Neilson, and A. Chraplyvy, "Fiber-optic transmission and networking: The previous 20 and the next 20 years," *Opt. Exp.*, vol. 26, 2018, Art. no. 24190.

[13] D. Marom et al., "Survey of photonic switching architectures and technologies in support of spatially and spectrally flexible optical networking," *J. Opt. Commun. Netw.*, vol. 9, pp 1–26, 2017.

[14] D. Klonidis et al., "Enabling transparent technologies for the developments of highly granular flexible optical cross-connects," in *Proc. IEEE Int. Conf. Transparent Opt. Netw.*, 2014, pp. 1–6.

[15] R. Rudnick et al., "Sub-GHz resolution photonic spectral processor and its system applications," *J. Lightw. Technol.*, vol. 35, pp 2218–2226, 2017.

[16] J. Xu et al., "Reciprocating reflective double gratings based LCOS spectral filter with sharp response," *J. Lightw. Technol.*, vol. 39, pp 3961–3966, 2021.

[17] S. Xiao and A. M. Weiner, "An eight-channel hyperfine wavelength demultiplexer using a virtually imaged phased-array (VIPA)," *IEEE Photon. Technol. Lett.*, vol. 17, no. 2, pp. 372–374, Feb. 2005.

[18] AJ. V. R. Metcalf, D. E. Supradeepa Leaird, and A. M. Weiner, "Fully programmable two-dimensional pulse shaper for broadband line-by-line amplitude and phase," *Opt. Exp.*, vol. 21, pp. 28029–28039, 2013.

[19] L.-M. Duan and C. Monroe, "Colloquium: Quantum networks with trapped ions," *Rev. Modern Phys.*, vol. 82, pp. 1–16, 2010.

[20] H-Series Quantinuum Roadmap, 2023. [Online]. Available: https://www.quantinuum.com/hardware/h1" https://www.quantinuum.com/hardware/h1

[21] D. Marpaung, J. Yao, and J. Capmany, "Integrated microwave photonics," *Nature Photon.*, vol. 13, pp 80–90, 2019.

[22] J. Wang et al., "Reconfigurable radio-frequency arbitrary waveforms synthesized in a silicon photonics chip," *Nature Commun.*, vol. 6, pp 1–8, 2015.

[23] S. Fatema, L. M. Cohen, N. B. Lingaraju, and A. M. Weiner, "Synthesis of narrowband spectral filters in active photonic multi-project wafer runs," in *Proc. IEEE Photon. Conf.*, 2022, pp. 1–2.

[24] V. Wankhade et al., "Low-loss, fine resolution wavelength-selective switch realized at a silicon photonics foundry," in*Proc. CLEO: Sci. Innov.*, 2023, Paper STu3J.6.

[25] Y. Bian et al., "Monolithically integrated self-aligned SiN edge coupler with $< 0.6/0.8$dB TE/TM insertion loss, < -39dB back reflection and >520mW high-power handling capability," in *Proc. Opt. Fiber Commun. Conf.*, 2023, Paper M3C.3.

[26] D. Onural, H. Gevorgyan, B. Zhang, A. Khilo, and M. A. Popovic, "Silicon waveguides and resonators with Sub-0.7 dB/cm propagation loss and over 7 million Q in a foundry process," in *Proc. Front. Opt.*, 2021, p. FTh6B–4.

[27] M. Popović, "Theory and design of high-index-contrast microphotonic circuits," Ph.D. Thesis, Dept. of Electrical Engineering and Computer Science, Massachusetts Institute of Technology, Cambridge, MA, USA, 2008.

[28] M. Bahadori et al., "Universal design of waveguide bends in silicon-on-insulator photonics platform," *J. Lightw. Technol.*, vol. 37, pp 3044–3054, 2019.

[29] N. M. Fahrenkopf, C. McDonough, G. L. Leake, Z. Su, E. Timurdogan, and D. D. Coolbaugh, "The AIM photonics MPW: A. highly accesible cutting edge technology for rapid prototyping of photonic integrated circuits," *IEEE J. Sel. Topics Quantum Electron.*, vol. 25, no. 5, pp 1–6, Sep./Oct. 2019.

[30] D. Onural, H. Gevorgyan, B. Zhang, A. Khilo, and M. A. Popović, "Ultra-high Q resonators and sub-GHz bandwidth second order filters in an SOI foundry platform," in *Proc. Opt. Fiber Commun. Conf. Exhib.*, 2020, pp. 1–3.

[31] G. H. Song and W. J. Tomlimson, "Fourier analysis and synthesis of adiabatic tapers in integrated optics," *J. Opt. Soc. Amer. A*, vol. 9, pp 1289–1300, 1992.

[32] B. E. Little et al., "Microring resonator channel dropping filters," *J. Lightw. Technol.*, vol. 15, no. 6, pp 998–1005, 1997.

[33] Z. Lu et al., "Performance prediction for silicon photonics integrated circuits with layout-dependent correlated manufacturing variability," *Opt. Exp.*, vol. 25, no. 9, pp. 9712–9733, 2017.

[34] T. Carmon, L. Yang, and K. J. Vahala, "Dynamical thermal behavior and thermal self-stability of microcavities," *Opt. Exp.*, vol. 12, pp 4742–4750, 2004.

[35] S. Singer et al., "Nonlinear loss and damage threshold in silicon photonic waveguides: Modelling and experimental verification," in *Proc. Conf. Lasers Electro-Opt.*, 2022, pp. 1–2.

[36] T. Akiba et al. 2019. [Online]. Available: https://optuna.org/

[37] O. Schwelb and I. Frigyes, "Vernier operation of series-coupled microring resonator filters," *Microw. Opt. Technol. Lett.*, vol. 39, pp 257–261, 2003.

[38] R. Boeck et al., "Series-coupled silicon racetrack resonators and the vernier effect: Theory and measurement," *Opt. Exp.*, vol. 18, pp 25151–25157, 2010.

[39] M. Watts et al., "Microring-resonator filter with doubled free-spectral-range by two-point coupling," in *Proc. Conf. Lasers Electro-Opt.*, 2005, pp. 273–275.

[40] W. Chen et al., "Flexible-grid wavelength-selective switch based on silicon microring resoantors with interferometric couplers," *J. Lightw. Technol.*, vol. 36, pp 3344–3353, 2018.

[41] S. Liu et al., "Thermo-optic phase shifters based on silicon-on-insulator platform: State-of-the-art and a review," *Front. Optoelectron.*, vol. 15, 2022, Art. no. 9.

[42] H. Jayatilleka et al., "Photoconductive heaters enable control of large-scale silicon photonic ring resonator circuits," *Optica*, vol. 6, pp 84–91, 2019.

[43] F. Morichetti et al., "ContactLess integrated photonic probe: Concept, technology, and applications," in *Proc. Opt. Fiber Commun. Conf. Exhib.*, 2016, pp. 1–3.

[44] D. De Aguiar et al., "Automatic tuning of silicon photonics microring filter array for hitless reconfigurable add-drop," *J. Lightw. Technol.*, vol. 37, pp 3939–3947, 2019.

[45] K. Padmaraj et al., "Wavelength locking and thermally stabilizing microring resonators using dithering signals," *J. Lightw. Technol.*, vol. 32, pp 505–512, 2014.

[46] C. Sun et al., "Single-chip microprocessor that communicates directly using light," *Nature*, vol. 528, pp 534–538, 2015.